2
A REVIEW OF THE LITERATURE

2.1 INTRODUCTION

Hardfacing is a complicated subject as it embraces aspects of welding technology, materials science and wear. While there have been many studies that focus on one or two of these particular aspects, few have dealt with all three. Consequently, this review addresses each aspect sequentially and draws on the relevant studies in each case. Sections 2.2 to 2.4 are concerned with various aspects of welding science, section 2.5 deals with the metallurgy of high-chromium white irons and section 2.6 addresses wear. Finally, section 2.7 outlines the rationale for the current work.

2.2 THE EFFECTS OF WELDING PARAMETERS ON DILUTION

2.2.1 Dilution – Its Definition and Significance

The ASM Handbook (1993a) defines dilution as:

"The change in chemical composition of a welding filler metal caused by the admixture of the base metal or previous weld metal in the weld bead. It is measured by the percentage of base metal or previous weld metal in the weld bead."

Dilution occurs when a volume of deposited filler material is mixed with a volume of substrate material. However, if dilution is to be measured by metallographic methods it is typically calculated in terms of a ratio of areas, as illustrated in Figure 2.1.

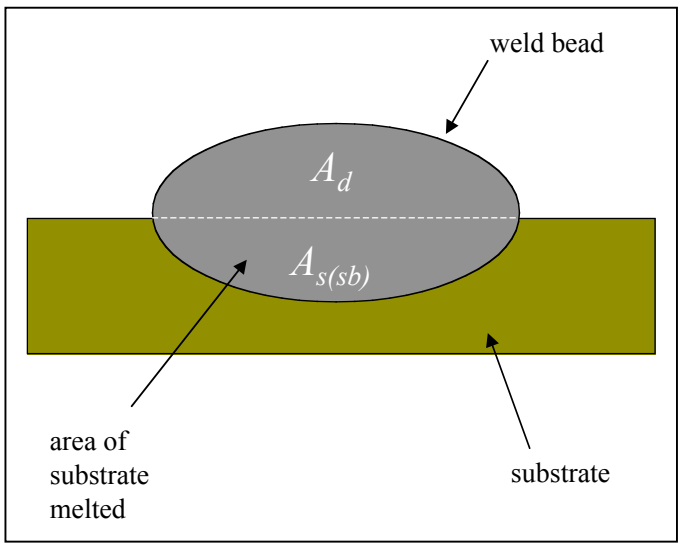

$$Dilution, \quad D_{sb} = \frac{A_{s(sb)}}{A_{s(sb)} + A_d} \quad (0 \leq D_{sb} \leq 1) \quad \ldots\ldots\ldots \quad (2.1)$$

Figure 2.1: - The metallographical measurement of dilution for a single-bead deposit. $A_{s(sb)}$ is the cross-sectional area of substrate melted and A_d is the cross-sectional area of material deposited.

This method of measurement is acceptable provided that the individual cross-sectional areas do not vary along the length of the weld.

Dilution is a parameter of prime importance because weld surfacing usually involves the joining of two materials with very different compositions. The substrate is often a steel containing 0.1-0.2 wt.% carbon and no chromium, whereas a typical welding consumable contains 5 wt.% carbon and 25 wt.% chromium. It can be seen that even a small change in dilution will result in a significant change in overlay composition, and hence microstructure and wear properties.

2.2.2 Previous Dilution Studies

It has long been known that the selected welding parameters affect the dilution and hence wear performance of high-chromium white iron overlays. Avery and Chapin (1952), in their study, made the following statement: *"The difference in performance due to welding technique is as great or greater than variations that can be assigned to (consumable) composition."* Despite this knowledge, there have been few studies investigating the role that welding parameters play in determining the overlay dilution. The most comprehensive studies were those of Thorpe (1980), Rense *et al.* (1983), Ellis and Garrett (1986) and Yellup and Smoker (1995). Each of these studies examined the effects of a range of different process variables. Rather than describe the findings in relation to individual parameters, a brief description is given of each study. A summary of the findings relating to each parameter is then given in Table 2.1. Trends in Table 2.1 are identified and explained with reference to the welding literature.

2.2.2.1 Thorpe (1980)

Thorpe prepared a range of three-layer deposits. The first layer of three beads was deposited with direct-current, electrode-positive polarity (DCEP), whereas the second layer, comprising two beads, and a third comprising one bead were both deposited with direct-current, electrode-negative polarity (DCEN). A 2.8mm diameter, self-shielding austenitic chromium-carbide-type consumable was used. A fully automatic flux-cored arc welding system was chosen to deposit the samples. It was found that dilution varied systematically with voltage but not with current. The effects of travel speed and work distance on dilution were also investigated.

Thorpe concluded that there was a trade-off between bead profile and the desired low-dilution microstructures.

2.2.2.2 Rense, Edwards and Frost (1983)

Heat input is a parameter of prime importance in many welding applications. Rense *et al.* (1983) selected combinations of parameters in such a way that they would detect any correlation between dilution and heat input. Each sample comprised a single-layer white iron overlay with overlapping beads. The voltage, current and travel speed were varied so that one of three heat input conditions were achieved, namely 1, 2 or 5kJ/mm. In this study it was found that there was no correlation between dilution and heat input, but that there was a correlation between dilution and current with an increase in current resulting in a reduction in dilution. However, the experimental design did not involve changing one parameter independently of another. The reduction in dilution observed by these workers could well have resulted from the simultaneous decrease in voltage (see Yellup and Arnold, 1996).

2.2.2.3 Ellis and Garrett (1986)

Ellis and Garrett reported work by Ellis (1985), who used factorial design to plan his experiments. The experiments included the deposition of sixty-four single beads on mild steel bars. The effects of such variables as arc polarity, voltage, current, travel speed, work distance and preheat temperature were considered. The welding consumable was 2.8mm in diameter, high in chromium but low in carbon. The major finding in this work was that there was an interaction between current and polarity in determining the dilution of the deposits. If DCEN polarity were used, increases in

current would result in reduced dilution. However, if DCEP polarity was used an increase in current resulted in a slight increase in dilution.

2.2.2.4 Yellup and Smoker (1995)

These workers used a 2.4mm diameter austenitic chromium-carbide-type consumable to deposit a range of multi-pass overlays. The effects of voltage, current, travel speed, torch angle and overlap were considered. Voltage was found to have the strongest effect on dilution with an increase in voltage leading to an increase in dilution. An increase in bead overlap was found to reduce the dilution in the case of multi-pass deposits.

2.2.2.5 Other Studies

Raveendra and Parmar (1987) and Martin *et al.* (1991) used factorial design techniques to study the geometry of single beads of steel deposited by flux-cored arc welding. They generated empirical equations for many parameters including dilution.

Kim, Basu and Siores (1994) studied single beads of steel deposited with the Gas-Metal Arc welding process (GMAW) and fitted their dilution data to an expression of the form:

$$D_{sb} = 10^{a_1} d^{a_2} S^{a_3} I^{a_4} V^{a_5}$$

where D_{sb} is the single-bead dilution, d is the diameter of the consumable, S is travel speed, I is current, V is voltage, and a_1, a_2, a_3, a_4 and a_5 are fitted constants. The effect that each parameter had on the dilution was inferred from the value of the index for that parameter.

Kalligerakis and Mellor (1994) studied overlay welding with stainless steel. The welding consumable was a 1.2mm diameter type 316 solid wire and the base metal was mild steel. The samples prepared by these workers comprised single beads-on-plate. Dilution was found to increase with increasing current.

Kotecki (1996) deposited a number of stainless steel overlays comprising overlapping beads with the submerged-arc welding technique. He found that by reducing the step-over between adjacent beads a very low dilution deposit could be achieved.

Table 2.1 summarises the findings of the major studies. For each welding parameter such as voltage or current, there is a box assigned to each publication. In each box there is an entry. An upward pointing arrow indicates that an increase in the welding parameter results in an increased dilution according to the findings of the study. Similarly, a downward pointing arrow indicates that an increase in the welding parameter will result in a reduction in dilution. If the entry is "~" the findings were inconclusive, or there was no noticeable trend, while "*N/C*" denotes that the particular parameter was not considered in the study.

2.2.3 The Effects of Voltage on Dilution

It can be seen that all of the studies that investigated the effect of voltage on dilution found that an increase in voltage resulted in an increase in dilution. This is in agreement with a first-principles model initiated by Deam (1996) and developed by Bednarz (1996). The resulting equation is described in Francis *et al.* (1998), where it was seen that the model described the single-bead dilution data obtained from two 2.8mm diameter chromium-carbide-type consumables. The equation is:

Study	Overlay Material	Voltage	Current	Work Dist.	Speed	Preheat Temp.
Thorpe (1980)	white iron	↑	~	□	~	*N/C*
Rense *et al.* (1983)	white iron	↑	□	*N/C*	*N/C*	*N/C*
Ellis and Garrett - DCEP (1986)	stainless steel	↑	↑	~	↑	↑
Ellis and Garrett - DCEN (1986)	stainless steel	↑	□	~	↑	↑
Raveendra and Parmar (1987)	steel	↑	□	□	*N/C*	*N/C*
Martin, Taylor and Bahrani (1991)	steel	↑	*N/C*	□	↑	*N/C*
Kim, Basu and Siores (1994)	steel	↑	□	*N/C*	↑	*N/C*
Kalligerakis and Mellor (1994)	stainless steel	*N/C*	↑	*N/C*	*N/C*	*N/C*
Yellup and Smoker (1995)	white iron	↑	~	*N/C*	~	*N/C*

Table 2.1: - A summary of the influence of welding parameters on dilution according to previous studies. In all cases the substrate materials were mild steel.

$$\frac{D_{sb}}{1 - D_{sb}} = \alpha \frac{VI}{W}\left(1 + \beta VIS\right) \quad \ldots\ldots\ldots \quad (2.2)$$

where D_{sb} is the single-bead dilution, V is the contact tip-to-work voltage, I is the current, W is the deposition rate, S is the travel speed and α and β are fitted constants depending on the combination of welding consumable and substrate. Equation 2.2 suggests that the single-bead dilution generally increases with increasing voltage.

DuPont and Marder (1996) also modelled single-bead dilution. They arrived at an expression of the form:

$$D_{sb} = \frac{1}{1 + \frac{V_{fm} E_s}{\eta_a \eta_m VI - E_{fm} V_{fm}}} \quad \ldots\ldots\ldots \quad (2.3)$$

where V_{fm} is the volume of filler metal deposited, E_s and E_{fm} are the changes in enthalpy required to melt substrate and filler metal respectively while η_a and η_m are the arc and melting efficiencies respectively. If it is assumed that the deposition rate, and hence V_{fm}, does not change with voltage (see Lesnevich, 1958), then D_{sb} in equation 2.3 monotonically increases with increasing voltage.

Farmer (1966a) described the effect that arc voltage has on single-bead dilution. An increase in voltage results in an increase in arc energy. The deposition rate, however, generally does not increase as the voltage increases. The increase in arc energy will result in more substrate being melted and, if the deposition rate does not increase, a higher dilution.

2.2.4 The Effects of Welding Current on Dilution

There are conflicting conclusions regarding the effect of welding current on single-bead dilution. Dilution depends on the amount of substrate melted as well as the amount of material deposited and welding current has an effect on both of these parameters. In order to appreciate how conflicting trends may arise it is necessary to consider the relationship between the current and the deposition rate. Lesnewich (1958) and Halmøy (1979) studied solid-wire GMAW and arrived at an expression of the form:

$$W = aI + blI^2 \quad \ldots\ldots\ldots \quad (2.4)$$

where W is deposition rate, I is current, l is work distance and a and b are constants depending on the wire diameter, electrode material and shielding gas. This form of expression has also been obtained by other workers (Rhee and Kannatey-Asibu, 1993; Hirata, 1995). Equation 2.4 suggests that the deposition rate is independent of the welding voltage. It is known, however, that deposition rate can vary with voltage in such a way that an increase in voltage causes a reduction in deposition rate (Kiyohara *et al.*, 1980). Nevertheless equation 2.4 does prove useful in estimating the deposition rate with both solid and flux-cored wires (Ushio *et al.*, 1985). If it is substituted into equation 2.2 the result is:

$$\frac{D_{sb}}{1 - D_{sb}} = \frac{V}{a + blI} + \frac{V^2 IS}{a + blI} \quad \ldots\ldots\ldots \quad (2.5)$$

The second term in equation 2.5 is monotonically decreasing in I and the third term is monotonically increasing. Equation 2.5 suggests that dilution could either increase or decrease with increasing current, depending on the term that dominates. Thus the Bednarz-Deam model for single-bead dilution appears to account for the seemingly contradictory findings in previous dilution studies. It suggests that the effects of welding current on single-bead dilution are not immediately evident, and that they will depend on the characteristics of the particular combination of substrate and consumable.

2.2.5 The Effects of Work Distance on Dilution

Three studies found that an increase in work distance resulted in a reduction in dilution. Thorpe (1980) concluded that the decreased dilution resulted from a reduction in arc voltage, due to an increase in the voltage drop between the contact tip and the tip of the electrode. Hinkel (1968) also acknowledged that there is a significant voltage drop associated with the electrode extension and estimated that it could be as high as 3 volts (V). French (1984) measured these voltage drops for flux-cored consumables and obtained values ranging from 0.5 to 4.5 volts (V); values which may be large enough to explain the observed reductions in dilution.

Another issue arises in that the work distance affects the deposition rate. Smith (1970) gave an example where the welding current could be reduced by 40%, while maintaining a constant deposition rate, by increasing the work distance from 25 to 95mm. The lower current will result in less substrate being melted and, since the deposition rate remains unchanged, a reduction in dilution. Conversely, if a constant current is maintained while the work distance is increased, there will be an increase in deposition rate according to equation 2.4. This will result in a larger cross-sectional area of deposited material and, since the amount of substrate melted will not increase, a lower dilution.

The only other work to consider the effect of work distance was that of Ellis and Garrett (1986). They found that there was no significant change in dilution as the work distance was changed. They did not, however, cover a wide range of work distances (see Ellis, 1985).

2.2.6 The Effects of Travel Speed on Dilution

Three of the studies found that dilution increases as the travel speed increases. In other work, Forsberg (1985) and Oh *et al.* (1990) also found that dilution increases with travel speed when cladding with strip electrodes. These findings are consistent with equation 2.2 and the Bednarz-Deam model for single-bead dilution.

The model developed by DuPont and Marder (see equation 2.3) does not directly suggest that an increase in travel speed results in an increase in dilution. However, the effect of travel speed may be accounted for by a change in the melting efficiency, η_m. DuPont and Marder define the melting efficiency as the ratio of energy used for melting to that which is delivered to the work piece. The melting efficiency has been shown to increase as the travel speed increases (Wells, 1952; Swift-Hook and Gick, 1973), and DuPont and Marder concluded that the increase in dilution with travel speed occurs as a direct result of the associated increase in melting efficiency.

2.2.7 The Effects of Preheat Temperature on Dilution

Ellis and Garrett (1986) considered the effects of preheat temperature. They found that an increase in preheat temperature resulted in an increase in dilution. Hotter substrates require less energy to reach their melting point. For a given heat input, an increase in preheat temperature will result in a greater amount of substrate material reaching the melting temperature. A higher dilution will result.

2.2.8 The Effects of Bead Overlap on Dilution

Yellup and Smoker (1995) and Kotecki (1996) both found that an increase in overlap, or a reduced step-over, resulted in reduced dilution for multi-pass single-layer deposits.

2.3 FACTORS AFFECTING WELD BEAD GEOMETRY

The prediction of weld bead geometry is an important step in the development of welding procedures. This section commences with a description of the analytical solutions for the temperature distribution in a weldment, and the weld bead geometry predicted by these solutions. The physical effects leading to discrepancies between the predicted and observed geometries are next to be addressed. Finally, some of the empirical correlations in the literature are discussed.

2.3.1 Studies Treating the Arc as a Point Source of Heat

Rosenthal (1941) was one of the first to present a solution for the temperature distribution in weldments. His solution applies to the case of a single bead being deposited on to a semi-infinite plate. The arc was assumed to be a point source of heat moving along the surface of the plate at a constant velocity. Physical properties such as density, specific heat and thermal conductivity were assumed to remain constant.

Christensen *et al.* (1965) generalised the early work of Rosenthal to arrive at a dimensionless temperature distribution for point sources. This distribution was compared with the results of experiments and measurements of weld pool geometry. The isotherm corresponding to the melting temperature of the material was the predicted fusion line. This isotherm is semi-circular and, as such, the predicted fusion line is a semi-circle. The predicted weld bead penetration is equal in magnitude to the radius of this semi-circle, whereas the predicted bead width is twice this value.

Christensen *et al.* found that there was good agreement between the predicted fused areas and those observed in experiment but, for most welding conditions, the weld bead

width was underestimated. They concluded that the semi-circular fusion line required by theory was not borne out in experiment.

2.3.2 Studies Treating the Arc as a Distributed Source of Heat

Rykalin (1951) acknowledged that the arc is a distributed source of heat. He argued that the arc produces heat at the cathode spot by direct conversion of the energy of electrically-charged particles into thermal energy. In addition, the region immediately adjacent to the cathode spot was said to receive thermal energy from the arc by convection and radiation. Rykalin pointed out that heating from the arc diminishes with increasing distance from the centre of the cathode spot and argued that the spatial distribution of heating could be approximated by the normal probability (or Gaussian) distribution.

Eagar and Tsai (1983) adapted Rosenthal's solution for the temperature distribution in a weldment and treated the heat flux from the arc as a Gaussian distribution. They demonstrated that, when predicting bead geometry, significant improvements over earlier models could be achieved. The depth-to-width ratios predicted by Eagar and Tsai achieved better agreement with experiment than the semi-circular fusion lines predicted by Rosethal (1941) and Christensen *et al.* (1965).

2.3.3 Weld Pool Convection and Its Effect

It is now known that the location of the fusion line is strongly influenced by convection in the weld pool (Kou and Wang, 1986). Fluid flow within the weld pool can result from surface tension gradients, the electro-magnetic force and the buoyancy force. The mechanism is described in each case.

2.3.3.1 Surface tension gradients

Heiple and Roper (1982) demonstrated the effects that surface tension gradients have on weld bead geometry. The gradients arise because there are temperature gradients within the weld pool and surface tension is a temperature-dependent property. If the surface tension within the weld pool decreases with increasing temperature (*i.e.* a negative gradient) the surface tension at the centre of the weld pool will be lower than at the periphery. The resulting convection pattern will be as shown in Figure 2.2(a). Heiple and Roper stated that it is normal for pure materials to exhibit a negative gradient. If, however, the surface tension of an alloy increases with increasing temperature (a positive gradient), the resulting convection pattern will be as shown in Figure 2.2(b). Heiple and Roper proposed that, for iron and steels, the presence of surface-active elements such as sulphur and oxygen produced a positive gradient.

A positive surface tension gradient favours the transfer of heat from the arc to the bottom of the pool thus producing deeper penetration. A negative surface tension gradient, however, retards the flow of metal from the top to the bottom of the pool and the resultant penetration is shallow (Kou and Wang, 1986).

2.3.3.2 The electro-magnetic force

The diverging electric current field in the weld pool creates a downward electro-magnetic force near the centre of the weld pool and pushes liquid metal in that region downward toward the bottom of the pool (Kou and Sun, 1985). Thus the electro-magnetic force favours a convection pattern such as that shown in Figure 2.2(b).

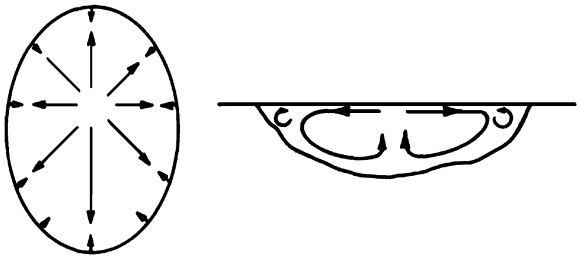

Figure 2.2(a): - Schematic representation of the flow pattern on the weld pool surface and the sub-surface flow pattern for a negative surface tension gradient (after Heiple and Roper, 1982).

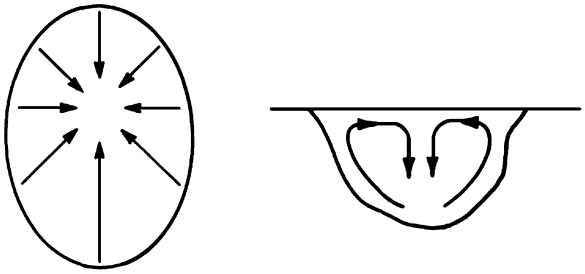

Figure 2.2(b): - Schematic representation of the flow pattern on the weld pool surface and the sub-surface flow pattern for a positive surface tension gradient (after Heiple and Roper, 1982).

2.3.3.3 Buoyancy

Under the influence of the buoyancy force the hotter liquid metal near the central region of the weld pool floats to the surface, while the cooler liquid metal near the pool boundary sinks to the bottom of the weld pool (Kou and Sun, 1985). Thus buoyancy effects favour a convection pattern such as that shown in Figure 2.2(a).

2.3.3.4 Combined driving forces

In arc welding there are several different driving forces for weld pool convection acting simultaneously. The convective flow direction will be governed by which driving force is dominant. However, it is possible for two flow loops of opposite directions to co-exist in a weld pool, the upper one being dominated by the surface tension gradient and the lower one by the electromagnetic force (Kou and Sun, 1985).

Kim and Na (1995) performed computer simulations of the 3-dimensional heat transfer and fluid flow within the weld pool for GMAW. In their work they calculated the position of the fusion line due to pure conduction with a distributed source of heat. They also calculated the location of the fusion line including the influences of three driving forces for convection; the electromagnetic force, surface tension and buoyancy. The results are shown in Figure 2.3.

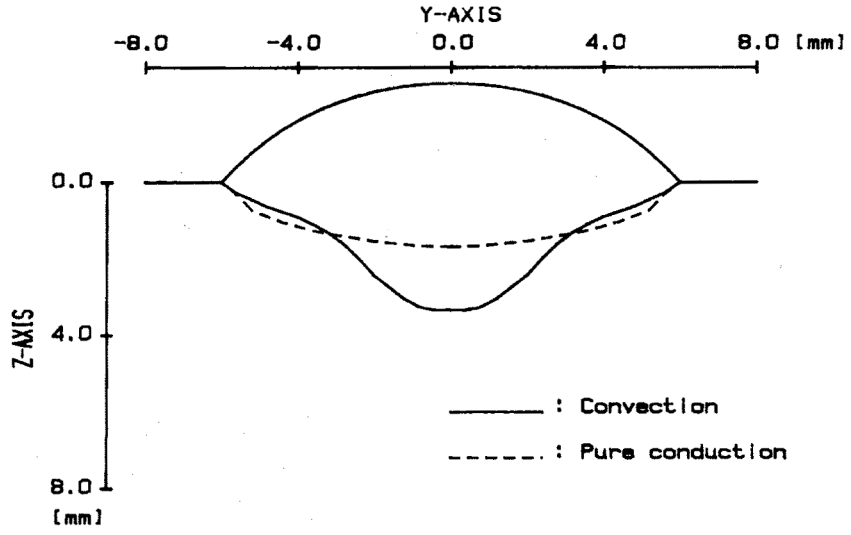

Figure 2.3: - A comparison of the calculated weld bead shapes for two different calculation methods (after Kim and Na, 1995). The electrode and substrate were both mild steel.

In section 2.3.1 it was noted that, for a point source of heat, the predicted fusion line was semi-circular. Figure 2.3 shows that pure conduction with a distributed source of heat produces a weld pool that is wider and approximately parabolic in shape. It is also evident that liquid metal flow plays an important role in the formation of the finger-like penetration profile frequently seen in GMAW welds. Kim and Na concluded that the electromagnetic force was the dominant driving force for liquid metal flow. They also found that the finger-like penetration profile was particularly prominent at low work distances. It was suggested that at low work distances the arc length is reduced and the current flux constricted, resulting in a large electro-magnetic force.

2.3.4 Weld Pool Depression and Its Effect

At high welding currents the surface of the molten weld pool becomes depressed, favouring transfer of heat from the arc to the root of the weld and producing a higher penetration (Friedman, 1978).

Friedman attributed the depression of the weld pool to the increase in arc pressure, since the force that the plasma jet imparts on the weld pool has been shown to increase with the square of the current (Lin and Eagar, 1986). However, Lin and Eagar (1985) in an earlier study, and later work by Rokhlin and Guu (1993) found that arc pressure alone could not explain the observed surface depression. Lin and Eagar developed a model of a compound vortex in the weld pool. This model did explain the surface depression and at the same time predicted a hysteresis in the relation between weld pool depression and current, the hysteresis being caused by vortex inertia. Hysteresis was not, however, observed by Rokhlin and Guu. Their results did not conclusively support the vortex model and they concluded that more work was required to explain the phenomenon of

weld pool depression. It was suggested that the electro-magnetic force, associated with the diverging current path in the weld pool, may play a significant role in the formation of the weld pool depression. This suggestion is supported by the work of Erokhin (1979), who suggested that there is no sense in separating the arc force from the electro-magnetic force in the plate. He measured the sum of these forces and obtained results that can explain weld pool depression.

2.3.5 Studies Considering the Effects of the Molten Droplets

Kim and Na (1995) considered the effects that the molten droplets travelling across the arc zone have on the shape of the weld pool. These effects were combined with those of a distributed source of heat, weld pool convection and depression. It was found that, when all of the influences were combined, a computer simulation could accurately predict the geometry of GMAW weld beads.

Kim and Na found that the inclusion of the molten droplets in the analysis resulted in an increase in penetration and an enhancement of the finger-like penetration profile. It should be noted, however, that the mode of metal transfer was assumed to be spray transfer. The effects of the molten droplets may vary if the transfer is globular, as is the case for most open-arc hardfacing consumables.

2.3.6 Prediction of Weld Bead Geometry

This section describes some empirical approaches for predicting weld bead geometry. All of the examples presented were derived from experiments involving a steel substrate and consumable. The parameters of main interest are penetration, and bead width and height. Work relating to each of these parameters will be considered separately.

2.3.6.1 Predicting penetration

McGlone (1982) in his review found that there was consensus in the literature regarding the effects of welding parameters on penetration. Penetration was primarily influenced by welding current, with an increase in current resulting in an increase in penetration. The work of Jackson and Shrubsall (1953) utilised an equation for penetration attributed to Gunnert. The equation combines the effects of voltage, V, current, I and travel speed S to predict penetration, p:

$$p = K \sqrt[3]{\frac{I^4}{S V^2}} \quad \text{.....} \quad (2.6)$$

where K is a constant depending on the characteristics of the welding process. This expression was obtained from samples deposited using the submerged-arc welding process.

Martin *et al.* (1991) examined the effects of welding parameters on the geometry of beads deposited by self-shielded flux-cored arc welding. They related the penetration, p, to the welding parameters with the following expression:

$$p = \text{constant} \times \frac{f^{1.213} \theta_g^{0.218}}{S^{0.096} l^{0.6}} \quad \text{.....} \quad (2.7)$$

where f is the wire feed rate, θ_g is the gun angle, S is the travel speed and l is the work distance. The strong dependence of penetration on current is evident in this case through the wire feed rate or deposition rate (see equation 2.4). The inclusion of other variables does, however, make it difficult to identify similar trends.

A different approach was adopted by Raveendra and Parmar (1987). They used fractional factorial techniques to develop mathematical models for predicting weld bead geometry. They considered the effects of voltage, current, travel speed, work distance and gun angle. This approach does consider a wide range of variables and possible interactions but leads to complicated relationships, such as the following twelve-term expression:

$$p = 3.487 + 0.356V + 0.338I - 0.400S - 0.088l - 0.356VI$$
$$- 0.181VS + 0.200V\theta_g + 0.181Vl - 0.388Il - 0.156S\theta_g + 0.244\theta_g l \quad \text{.....} \quad (2.8)$$

where V is voltage, I is current, S is speed in mm/min, l is work distance in mm and ϕ_g is the gun angle in degrees.

2.3.6.2 Predicting bead width

Martin *et al.* (1991) and Kim *et al.* (1994) found that voltage was the dominant influence on bead width, with an increase in voltage resulting in an increase in bead width. Both of these works also found that an increase in travel speed resulted in a reduction in bead width. Raveendra and Parmar (1991) found that an increase in current increases the bead width, as did Kim *et al.* (1994).

Kim *et al.* (1991) obtained the following expression for bead width, w:

$$w = d^{0.3647} S^{-0.4873} I^{0.4151} V^{0.9273} \times \text{constant} \quad \text{.....} \quad (2.9)$$

where d is the consumable diameter, S is the travel speed, I is the welding current and V is the voltage.

Another expression was obtained by Martin *et al.* (1991):

$$w = \text{constant} \times \frac{V^{1.243} f^{0.221}}{S^{0.545} l^{0.09} \theta_g^{0.046}} \quad \cdots\cdots\cdots (2.10)$$

where V is voltage, f is wire feed rate, S is travel speed, l is work distance and θ_g is the gun angle.

2.3.6.3 Predicting bead height

Raveendra and Parmar (1987) and Kim *et al.* (1994) found that bead height increases with increasing current, while it decreases with increasing voltage and increasing speed. These findings agree with the work of Martin *et al.* (1991) who arrived at the following expression for bead height, h:

$$h = \text{constant} \times \frac{f^{0.933} \theta_g^{0.25}}{V^{0.417} S^{0.263} l^{0.239}} \quad \text{.....} \quad (2.11)$$

where f is the wire feed rate, θ_g is the gun angle, V is the voltage, S is the travel speed and l is the work distance. The strong dependence of height on welding current is evident through the dependence on wire feed rate.

Unfortunately, with the wire feed rate as a variable, there is an implicit dependence on the consumable type. For the same wire feed rate, the deposition rate will change if the consumable diameter is changed.

Kim *et al.* (1994) also produced an expression for bead height:

$$h = d^{-0.4092} G^{-0.0844} S^{-0.4327} I^{0.7475} V^{-0.6649} \times \text{constant} \quad \text{.....} \quad (2.12)$$

where d is the electrode diameter, G is the gas flow rate, S is the travel speed, I is current and V is voltage. Both equations 2.11 and 2.12 predict that an increase in current will increase bead height and that increases in voltage and speed will reduce bead height.

2.4 HOMOGENEITY OF THE WELD BEAD

In continuous welds involving the deposition of filler material it is possible for macro-segregation to occur if mixing in the weld pool is insufficient. In arc welding, however, the electromagnetic force tends to promote bulk mixing within the weld pool (Kou and Wang, 1986). Even if double circulation loops are present, due to the combined action of different driving forces, it is anticipated that they will not prevent bulk mixing within the weld pool. The kinetic energy of the molten droplets, together with the force of gravity, will ensure that they are drawn into the lower circulation loop induced by the electro-magnetic force (Kou and Wang, 1986). These concepts are consistent with the findings of Houldcroft (1954), who observed a uniform composition in the bulk fusion zone of aluminium welds made with dissimilar filler materials. Kou and Wang (1986) did point out, however, that the velocity of the liquid metal at the pool boundary should be zero. They suggested that a thin unmixed layer of material would result adjacent to the interface, and noted that such an unmixed zone had been reported by Baeslack *et al.* (1979) and Lippold and Savage (1980). The unmixed zone so formed is represented schematically in Figure 2.4.

Powell (1979) studied hardfacing deposits, employing the manual-metal-arc technique, and identified a possible cause of inhomogeneity. He observed that in some instances there were undissolved particles of ferrochromium present in the deposit. It is possible that, under certain conditions, ferrochromium particles in the welding consumable do not

completely melt as they travel across the arc zone. Thorpe (1980) also observed some undissolved ferrochromium particles in his samples, but to a lesser extent. Thorpe employed FCAW and attributed the reduced occurrence to the higher heat input of this process. Noble (1985), in his review, suggested that another possible cause was variations in ferrochromium particle size between MMA and FCAW consumables.

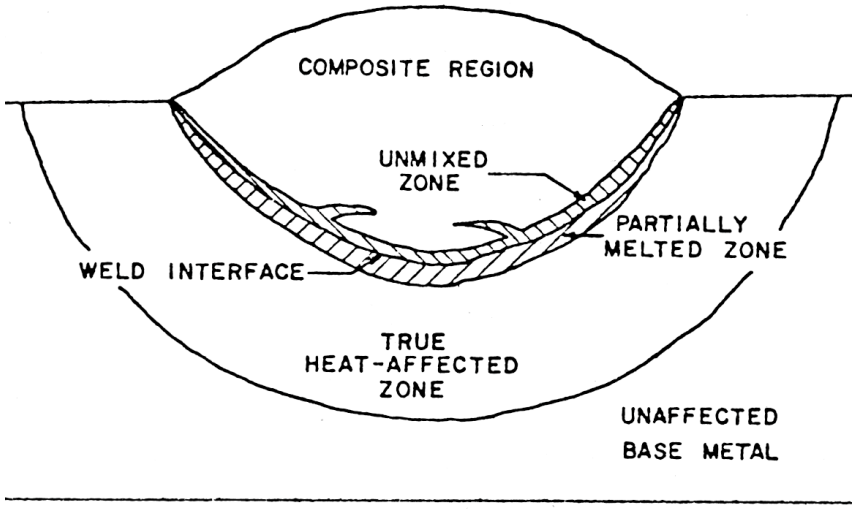

Figure 2.4: - Schematic illustration showing the regions of a heterogeneous weld (after Baeslack and Savage, 1979).

2.5 THE METALLURGY OF HIGH-CHROMIUM WHITE IRONS

In this section a brief description is given of the microstructures frequently observed in hardfacing weld deposits, and how they arise. The Fe-Cr-C liquidus surface is an appropriate starting point when studying the metallurgy of high-chromium white irons. The equilibrium phase diagram is described by Rivlin (1984) but, due to the rapid cooling rates associated with arc welding, the metastable liquidus surface proposed by Thorpe and Chicco (1985) or Jackson (1970) is more appropriate. A recent study (de

Sairre Balsamo *et al.*, 1995) found that the diagram proposed by Jackson (1970) adequately predicted weld-deposited high-chromium white iron microstructures. Jackson's diagram is shown in Figure 2.5.

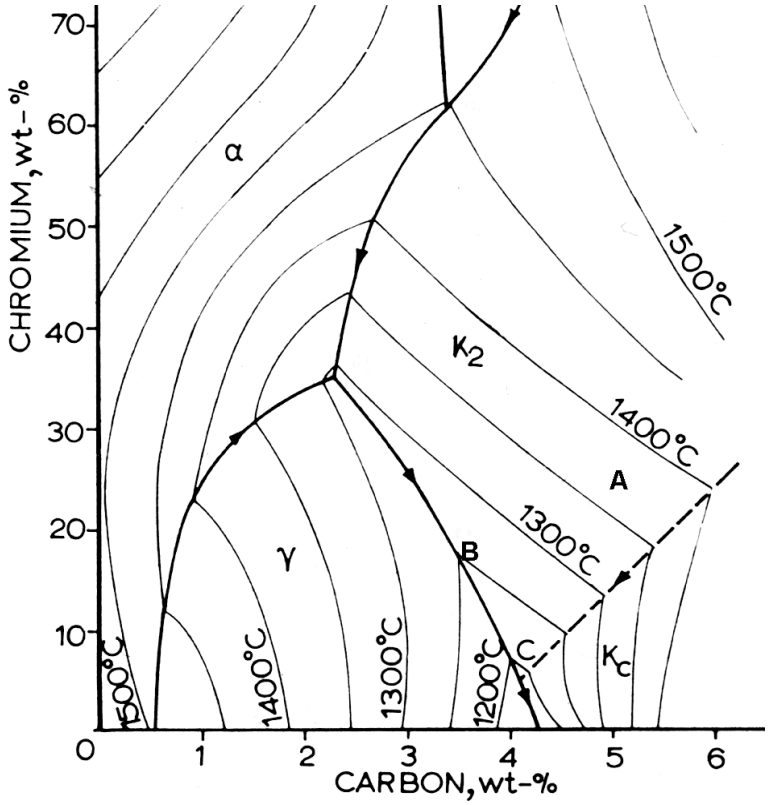

Figure 2.5: - The metastable Fe-Cr-C liquidus surface (after Jackson, 1970). K_c represents the $(Fe,Cr)_3C$ carbide and K_2 represents the $(Cr,Fe)_7C_3$ (or M_7C_3) carbide phase.

Many open-arc hardfacing consumables produce an all-weld-metal deposit with approximately 25 wt.% chromium and 5 wt.% carbon. A typical all-weld-metal composition is denoted "A" in Figure 2.5. The substrate is usually mild steel, containing no chromium and approximately 0.1-0.2 wt.% carbon. For the purposes of this illustration the substrate can be considered to be at the origin in Figure 2.5. As an

overlay is deposited, the weld pool is host to a mixing process between molten globules at the all-weld-metal composition (*i.e.* at "A") and molten substrate material (at the origin). The average composition of the bead will lie on the straight line between the origin and "A", with the exact point being determined by the dilution of that bead. "B" represents a point on the line "OA". If the dilution is high, the composition will fall to the left of "B" and a hypoeutectic microstructure will result. The microstructure will comprise primary dendrites of austenite (in Figure 2.5) in a eutectic mixture of austenite and carbide. The austenite may subsequently transform to martensite on cooling. A hypoeutectic microstructure is shown in Figure 2.6(a). If the composition falls on point "B" the microstructure will be entirely eutectic (Figure 2.6(b)). Finally, if the dilution is low, and the composition falls between "B" and "A", the microstructure will be hypereutectic, comprising needles of primary $(Cr,Fe)_7C_3$ carbide in a eutectic mixture of austenite (or martensite) and carbide. A hypereutectic microstructure is shown in Figure 2.6(c).

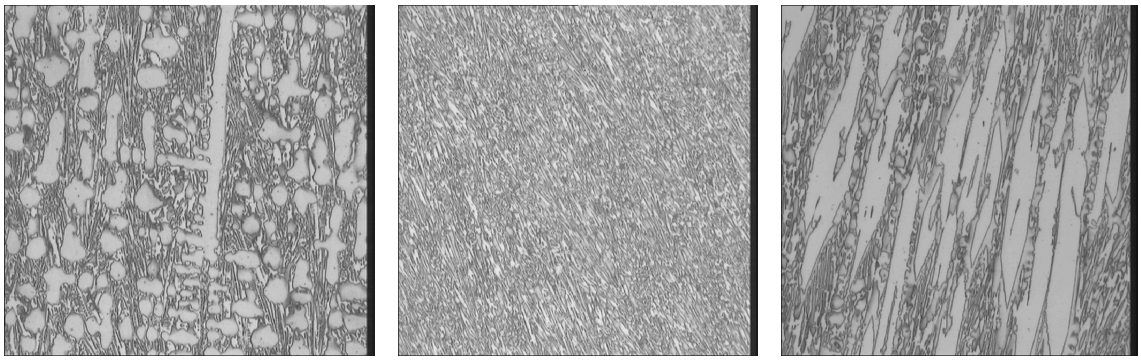

(a) **(b)** **(c)**

Figures 2.6: - Hypoeutectic (a), eutectic (b) and hypereutectic (c) microstructures respectively (after Francis and Jones, 1997).

If, at low levels of dilution, a welding consumable produces a hypereutectic deposit, it is generally referred to as a chromium-carbide-type consumable. These consumables are

further classified according to the structure of the matrix constituent in the eutectic. The matrix is usually either austenite, martensite or a combination of the two. All of the welding consumables used in the current work were of the chromium-carbide-type.

Powell (1979) studied hardfacing weld deposits and observed that the primary carbides in hypereutectic deposits were hollow and hexagonal in cross-section. Thus they could appear as either needle-like rods or hexagonal platelets depending on the orientation of their axes relative to the plane of polish. Powell noted that the carbides were usually aligned parallel to the direction of heat flow, which is roughly perpendicular to the base plate. However, he also observed that carbides could nucleate and grow in non-uniform orientations from any undissolved particles of ferrochromium present in the deposit.

There is a microstructural variation in hypereutectic white irons, namely the complex regular structure (Powell *et al.*, 1997). Fast cooling rates, and the presence of either silicon or boron, promote undercooling and a change in carbide morphology from that in a normal hypereutectic deposit to that of an undercooled alloy (Powell *et al.*, 1994). Under these circumstances it is not possible to distinguish primary and eutectic carbides as the morphology is continuous (Powell *et al.*, 1994).

2.6 THE ABRASIVE WEAR OF HIGH-CHROMIUM WHITE IRONS

This section describes abrasive wear and some of the factors affecting the abrasive wear resistance of high-chromium white irons.

2.6.1 Definitions and Types of Abrasive Wear

Czichos (1978) gave the following description of abrasive wear:

"The effect of abrasion occurs in contact situations in which direct physical contact between two surfaces is given where one of the surfaces is considerably harder than the other. The harder surface asperities press into the softer surface with plastic flow of the softer surface occurring around the asperities from the harder surface. When a tangential motion is imposed the harder surface will move, ploughing and removing the softer material."

Abrasion is usually categorised by the type of contact, with the two categories being two-body and three-body abrasion. The former occurs when an abrasive slides along a surface and the latter when the abrading particles are caught between one surface and another (ASM Handbook, 1992).

Avery (1961) further categorised abrasion by describing three distinct types, namely scratching (or low-stress) abrasion, grinding (or high-stress) abrasion and gouging abrasion. Low-stress abrasion generally involves small abrasive particles, low stress levels and no impact. High-stress abrasion involves small to medium-sized abrasive particles, high stress levels, but no impact. Finally, gouging abrasion is associated with large abrasive particles, very high stress levels and impact.

The ASM Handbook (1992) gives a different description of the three categories of abrasion. Low-stress abrasion occurs when the abrasive remains relatively intact, an example being the sanding of wood with sandpaper. High-stress abrasion occurs when the abrasive particles are being crushed, such as in a ball mill where both the grinding balls and ore are worn down. Finally, gouging abrasion exists when a relatively large abrasive cuts the material without full work hardening occurring, such as is the case where rocks are comminuted in a jaw-crusher.

2.6.2 The Relation Between Abrasive Wear Resistance and Hardness

It is known (Krushchov, 1957; Richardson, 1967; Moore, 1974) that there is a strong correlation between the apparent abrasive wear resistance of a material and its hardness, with a higher hardness resulting in better wear performance. Indeed, high-chromium white irons are widely used to combat abrasive wear due to the presence of hard $(Cr,Fe)_7C_3$ carbides in the microstructure (ASM Handbook, 1993b). It should be noted, however, that hardness does not always provide a reliable indication of the abrasive wear performance of a material, a fact that was well demonstrated by Cookson (1982). It is also known that abrasive wear resistance is not an intrinsic property of a material as it depends on the wear system (Czichos, 1977).

2.6.3 The Influence of Carbide Volume Fraction on Abrasive Wear Performance

Carbide volume fractions play an important role in determining the abrasion resistance of a white iron. Sare (1979), for example, reported that the low-stress abrasion resistance of white cast irons is principally controlled by the carbide volume fraction. There are two volume fractions used in the literature. The first will be referred to as the total carbide volume fraction *(TCVF)*, which embraces both eutectic and primary carbides. The second is the primary carbide volume fraction *(PCVF)*, which is relevant only for hypereutectic deposits. The *PCVF* distinguishes the large needle-like primary carbides from the finer eutectic carbides.

Rense *et al.* (1983) conducted one of the few studies that examined the relationship between the total carbide volume fraction and the abrasive wear performance of weld

deposits. These workers performed dry-sand/rubber-wheel abrasion tests on their samples. (This test is considered to be representative of low-stress abrasion.) It was found that the abrasion resistance improved rapidly with increasing total carbide volume fraction and with increasing heat input. The correlation with heat input was thought to be related to the coarseness of the microstructure.

Yellup and Smoker (1995) performed pin-abrasion tests on their weld deposits using the method described by Muscara and Sinnott (1972). This test is considered to fall in the category of high-stress abrasion. Yellup and Smoker found that, for hypoeutectic deposits, the wear rate improved as the volume fraction of eutectic carbides increased. The improvement in wear performance was much greater, however, in hypereutctic deposits when the volume fraction of primary carbides was increased.

Zum Gahr and Eldis (1980) performed pin-abrasion tests on samples taken from high-chromium white iron castings. They cast thirteen different alloys with total carbide volume fractions ranging from 7 to 45%. When 150-mesh garnet was used as the abrasive, the wear rate decreased monotonically with increasing *TCVF*. However, when silicon carbide was used as the abrasive, higher carbide volume fractions produced higher wear rates. Zum Gahr and Eldis argued that higher carbide volume fractions lead to better abrasion resistance provided that the abrading particles are softer than the M_7C_3 carbides. This generally applies when garnet and quartz are the abradants. If, however, the abrading particles are harder than the M_7C_3 carbides, as is the case with silicon carbide particles, higher carbide volume fractions may result in little benefit or even a reduction in abrasion resistance. It was argued that silicon carbide particles were able to

penetrate and crack the M_7C_3 carbides, resulting in spalling of the sample. Zum Gahr and Eldis' data are plotted in Figure 2.7.

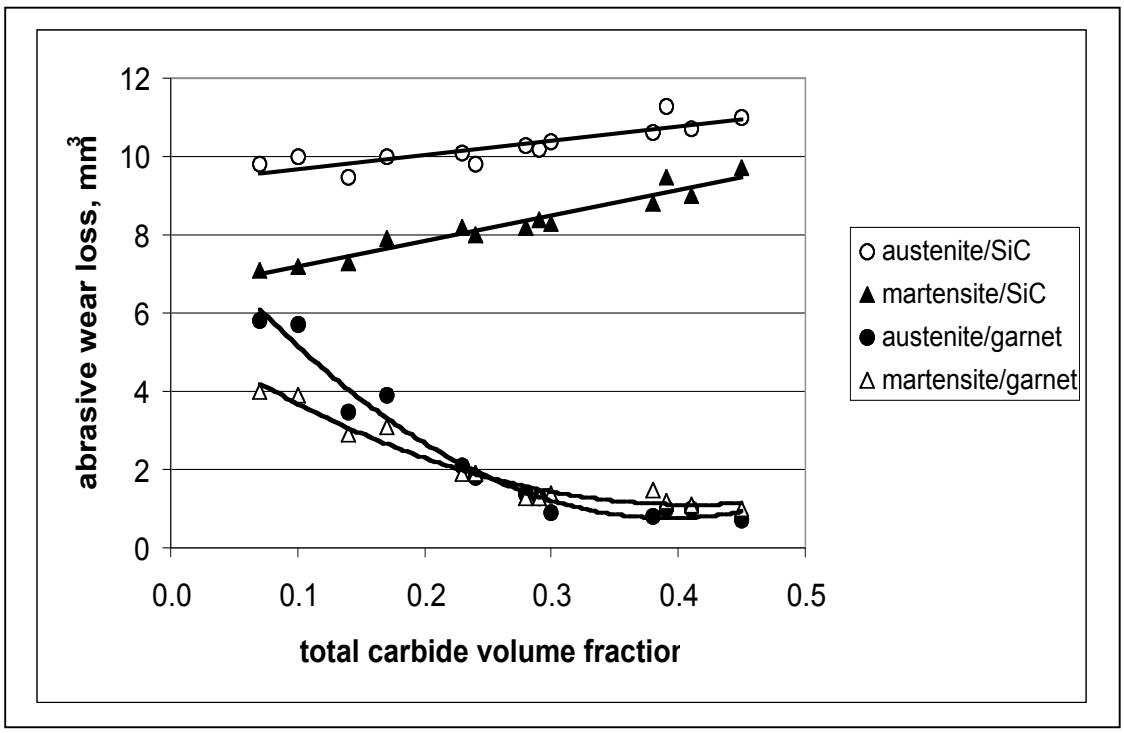

Figure 2.7: - Abrasive wear loss as a function of the total carbide volume fraction (after Zum Gahr and Eldis, 1980). The abrasive materials were 180-grit silicon carbide and 150-grit garnet. The matrices were either predominantly austenitic or predominantly martensitic.

According to Gundlach and Parks (1978), quartz and garnet are representative of the abrasives most commonly encountered in service in the minerals processing industry. It is expected, therefore, that high-chromium white irons with high carbide volume fractions will generally provide excellent resistance to low- and high-stress abrasion in many industrial applications. There are, however, instances in which high carbide volume fractions do not provide optimum wear resistance. Zum Gahr and Doane (1980) and Fulcher *et al.* (1983) provide examples in which the optimum wear performance is achieved at intermediate carbide volume fractions, near the eutectic composition. In these cases the alloys with high carbide volume fractions wear at faster rates due to

spalling of the primary carbide needles (Fulcher *et al.*, 1983). There are other factors that also play a role in determining the abrasion resistance of a material, such as the mean free path and the average distance between carbide particles (Sare, 1979). The orientation of the carbide needles has also been shown to be significant (Dogan and Hawk, 1995).

2.6.4 The Influence of Matrix Structure on Abrasive Wear Performance

Very few studies have specifically investigated the influence of matrix structure on the abrasive wear performance of hardfacing weld deposits. However, some workers have studied the role played by the matrix in white iron castings (Sare, 1979; Zum Gahr and Doane, 1980). These studies have found that the matrix plays an important role in supporting the M_7C_3 carbides, with the carbides being the dominant influence on the abrasion resistance of the alloy. Austenitic matrices were found to provide a higher fracture toughness and result in a higher resistance to spalling. Sare (1979) found that an austenitic matrix also led to improved abrasion resistance. Zum Gahr and Doane (1980), however, and Zum Gahr and Eldis (1980) found that martensitic matrices provided better resistance to abrasive wear and that, if only a moderate fracture toughness were required, martensitic matrices were the preferred choice.

2.6.5 Check Cracking in Hardfacing Overlays

Open-arc hardfacing involves the joining of two dissimilar materials. High-chromium white iron overlays have a different coefficient of thermal expansion to steels and, due to their limited ductility, usually develop check cracks (Farmer, 1974). It is generally believed in the Australian hardfacing industry that coarser check crack distributions, which result when a high heat input is employed, are deleterious to wear performance

(Gorman, 1997). Larger check cracks are believed to increase the likelihood of spalling. This belief has also emerged elsewhere, as evidenced by the filing of a patent covering the use of low heat input welding techniques as a method of achieving a fine check crack distribution (Ashida *et al.*, 1994). The patent covers heat inputs in the range 0.2 to 0.6 kJ/mm. There do not, however, appear to be any quantitative studies in the literature dealing specifically with the effects of check cracking on the abrasive wear performance of hardfacing overlays.

2.6.6 A Quantitative Approach to the Abrasive Wear of Composite Materials

Zum Gahr (1987) presented a quantitative approach to the abrasive wear of composite materials. He pointed out that wear resistance was known not to be a material property, since it depends on the characteristics of the wear system (Czichos, 1977). However, it was demonstrated that there are identifiable upper and lower limits for the abrasive wear rates of a composite if the wear rates of each constituent are known.

Zum Gahr considered a composite material to comprise a matrix phase and a reinforcing phase. The upper and lower bounds for wear rates are then obtained from linear and inverse rules of mixtures. For a given wear system, if the wear rates of the matrix phase and reinforcing phase are W_1 and W_2, then the wear resistances are W_1^{-1} and W_2^{-1} respectively. If both phases in the composite wear simultaneously then the wear resistance of the composite, W_c^{-1}, is given by the linear rule of mixtures, *i.e.*:

$$W_c^{-1} = \frac{1}{\frac{v_1}{W_1^{-1}} + \frac{v_2}{W_2^{-1}}} \quad \text{.....} \quad (2.13)$$

where v_1 and v_2 are the volume fractions of the matrix and reinforcing phases respectively. Conversely, if each phase wears sequentially the wear resistance of the composite material is described by an inverse rule of mixtures, *i.e.*:

$$W_c^{-1} = v_1 W_1^{-1} + v_2 W_2^{-1} \quad \text{.....} \quad (2.14)$$

Zum Gahr tested his own pin-abrasion data (described in Zum Gahr and Eldis (1980)), and observed that the wear rates fell between his predicted upper and lower limits. His results are represented graphically in Figure 2.8.

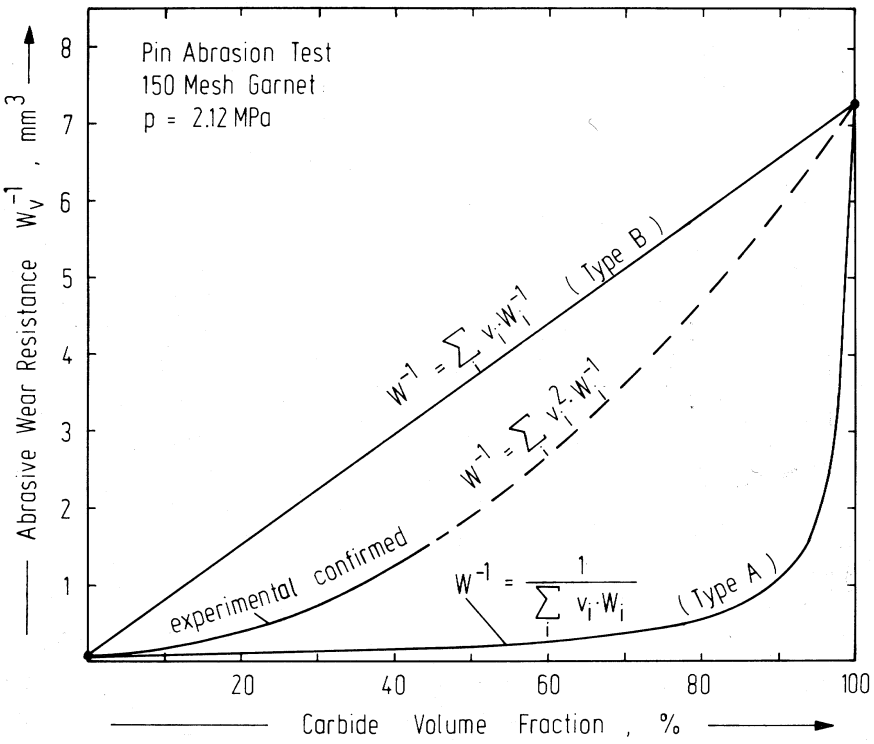

Figure 2.8: - A graphical representation of the upper and lower limits for abrasive wear of composite materials after Zum Gahr (1987). Type A systems involve simultaneous wear only, whereas Type B systems correspond to sequential wear. The intermediate curve corresponds to the data described in Zum Gahr and Eldis (1980). p is the contact pressure at the interface between the pin and the abrasive cloth.

2.7 THE RATIONALE FOR THE CURRENT WORK

There are many publications in the literature dealing with microstructure/wear relationships for high-chromium white irons. These works include two recent Ph.D theses (Stevenson, 1995; Tabrett, 1997), the first of which dealt with microstructures in hardfacing weld deposits. By comparison, few publications deal with the relationship between welding parameters and microstructure. Stevenson, in his conclusions and suggestions for further work, stated that the effect of welding parameters had not been studied. It was intended that the current work address this issue.

It was seen in section 2.2 that there are apparent discrepancies between the findings of various dilution studies but, with some analysis, it was possible to identify consistent trends. An interesting point arises, however, in that most of the published work relates to single-bead deposits. Unfortunately, many (if not most) hardfacing applications require complete surface coverage, *i.e.* a multi-pass overlay. It is not yet clear whether the trends observed in section 2.2 also apply to multi-pass overlays. This issue needs to be clarified and any differences between the two types of deposits need to be identified.

The prediction of parameters such as single-bead width, height and penetration is a necessary step in the development of welding procedures. It was seen in section 2.3 that there are many influences on these parameters and that the prediction of weld bead geometry is not a trivial task. All of the methods described in the literature are empirical approaches and, unfortunately, the resulting expressions are cumbersome. There is a great need to examine the possibility of first-principles analyses, as they may result in a unified approach to a wide range of materials and properties.

Very few workers have investigated the relationship between the microstructure of a weld deposit and its wear performance. There is a need to establish whether or not the trends that have been identified by Zum Gahr and other workers (see Zum Gahr and Eldis, 1980) for white iron castings also apply to weld deposits. The wear performance of weld deposits will ultimately dictate guidelines that may be developed for the deposition of optimum high-chromium white iron overlays.